Supplementary Materials for

Stable ultrafast graphene hot-electron source on optical fiber

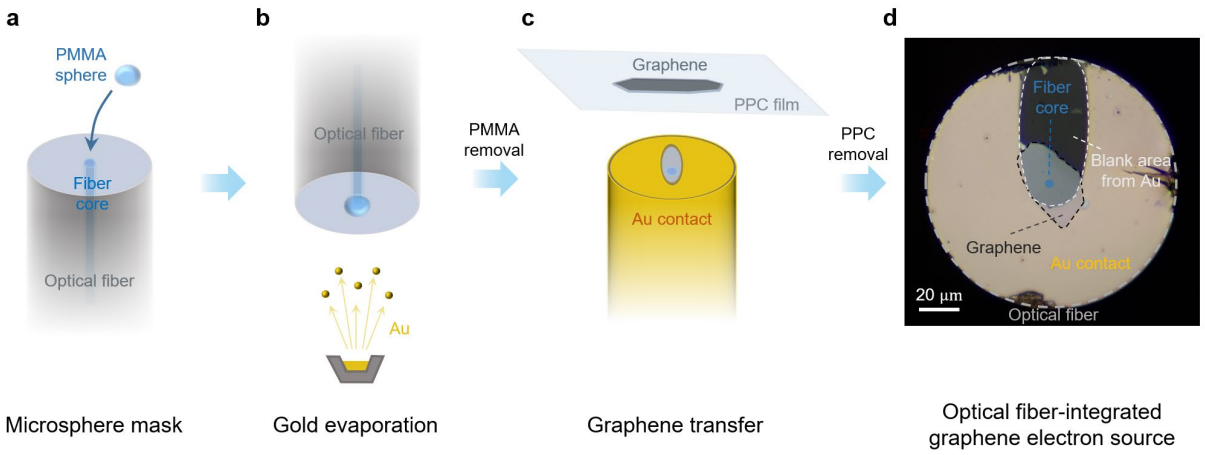
Guangjie Yao, Hao Hong, Xu Zhou, Kaifeng Lin, Huazhan Liu, Yilong You, Chang Liu, Ke Chen, Chi Li, Jianbo Yin, Zhujun Wang, Xuewen Fu, Qing Dai, Dapeng Yu and Kaihui Liu

The supplementary information includes:

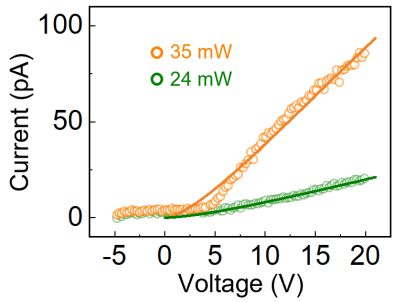
Supplementary Figures 1-14

Supplementary Table 1, 2

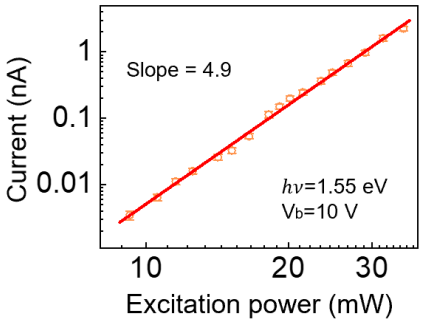
Supplementary Note 1, 2



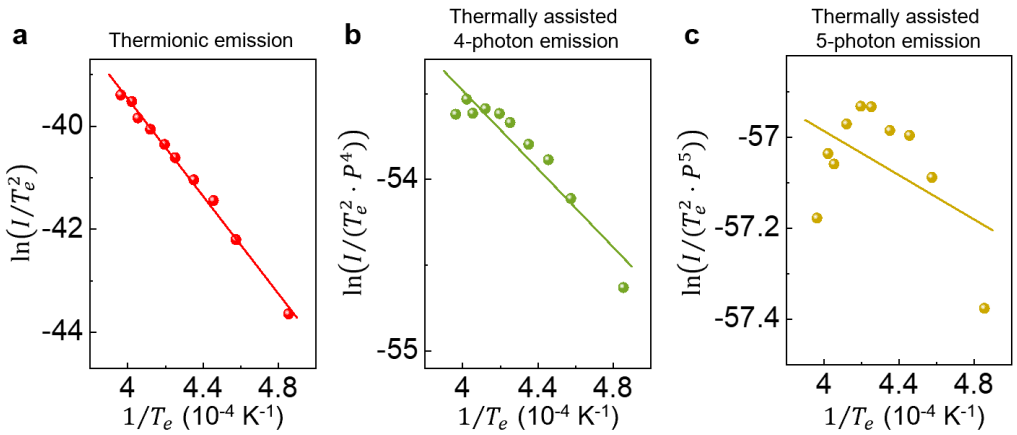
Supplementary Figure 1 | Schematics for the preparation of graphene electron source integrated on optical fiber. a, A PMMA (polymethyl methacrylate) microsphere is placed at the center of optical fiber as mask. **b,** After electron beam deposition of 5 nm Pd and 60 nm Au film, PMMA microsphere is dissolved into acetone leaving an exposed optical fiber core. **c,** A mechanically exfoliated graphene on PPC (polypropylene carbonate) film is transferred onto the optical fiber end face using a home-made optical fiber transfer stage. **d,** Optical microscope image of fabricated optical fiber-integrated graphene.



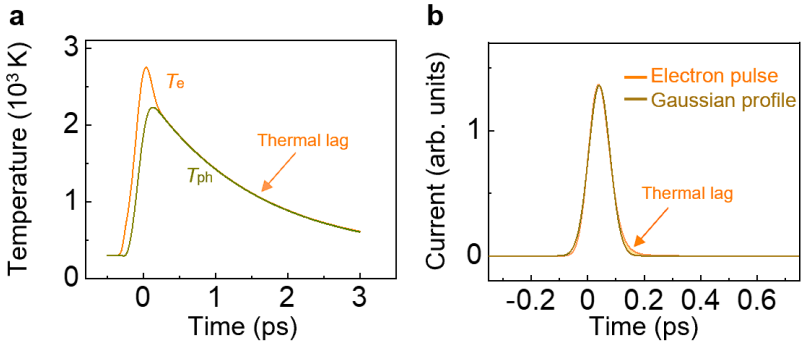
Supplementary Figure 2 | Longo equation fitting of voltage dependent emission current. The I-V curves (circles) with 24 mW and 35 mW excitation (corresponding to 2300 K and 2520 K in Fig. 1d, respectively) is fitted with Longo equation (solid lines): $I_{\mathrm{tot}} = \frac{I_{\mathrm{SC}} I_{\mathrm{TL}}}{I_{\mathrm{SC}} + I_{\mathrm{TL}}}$. I_{tot} is total current, $I_{\mathrm{SC}} = K \cdot U^{\frac{3}{2}}$ is the space charge current, $I_{\mathrm{TL}} = I_{\mathrm{S}} \cdot \exp\left(\frac{4.4}{T} sqrt\left(\frac{U}{d}\right)\right)$ is temperature limited current. K is a constant, U is applied voltage, I_{S} is the saturated current, T is cathode temperature and d is distance between anode and cathode. The fittings give a derived saturated current (I_{S}) of 44 pA and 154 pA, respectively.



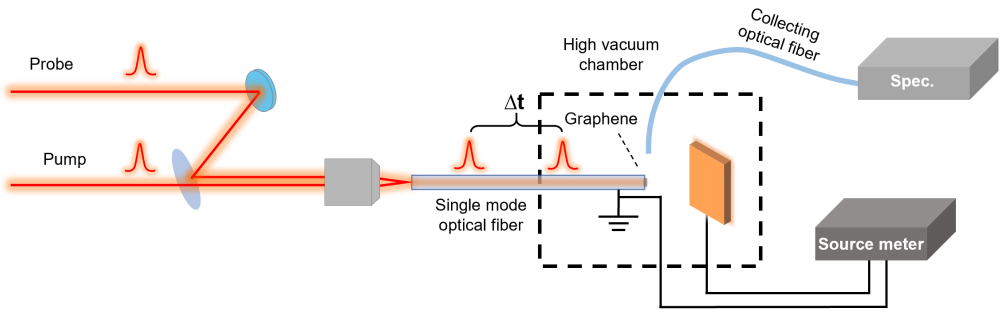
Supplementary Figure 3 | Emission current as a function of excitation power for 1.55 eV photon energy excitation. Power dependence order shows a similar value of ~4.9. The error bars are from standard deviation across about averaging 300 points. All data is obtained via optical fiber excitation. As a semimetal, graphene holds special Dirac cone band structure. This characteristic band structure with Dirac fermions gives a typical constant absorption (~2.3% for monolayer) over a broad wavelength range (from visible to near-infrared). For the hot electron process, the total absorbed photon energy directly determines the up-converted energy of electrons and holes thermal distribution (i.e., the quasi-equilibrium temperature). And the temperature is the most important parameter to describe the thermalization and relaxation processes as well as the electron emission process. As a result, laser excitations at different wavelengths hardly influence the hot electron behaviour of graphene within a wide bandwidth.



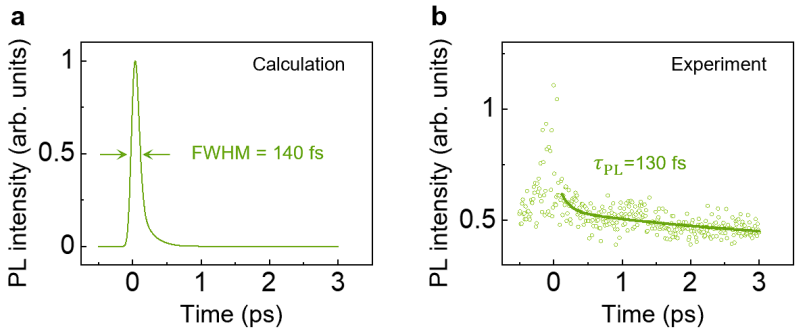
Supplementary Figure 4 | Behaviours of thermionic emission and thermally assisted multi-photon emission. a, Thermionic emission R-D model. **b,** Thermally assisted 4-photon emission. **c,** Thermally assisted 5-photon emission. The fitting is based on modified Fowler-Dubridge (F-D) theory[1] to describe the thermally assisted multi-photon emission as: $\ln\left(\frac{I_n}{T_e^2 \cdot P^n}\right) = \frac{nh\nu - \phi}{k_B} \cdot \frac{1}{T_e} + \ln(A_n)$. I_n is the electron emission current involving n photons, A_n is a constant, P is the incident laser intensity, T_e is the electron temperature, ϕ is the work function, k_B is Boltzmann constant, $h\nu$ is the laser photon energy. The thermionic emission model provided the best fit. Thus, the mechanism of thermally assisted multi-photon emission can be excluded.



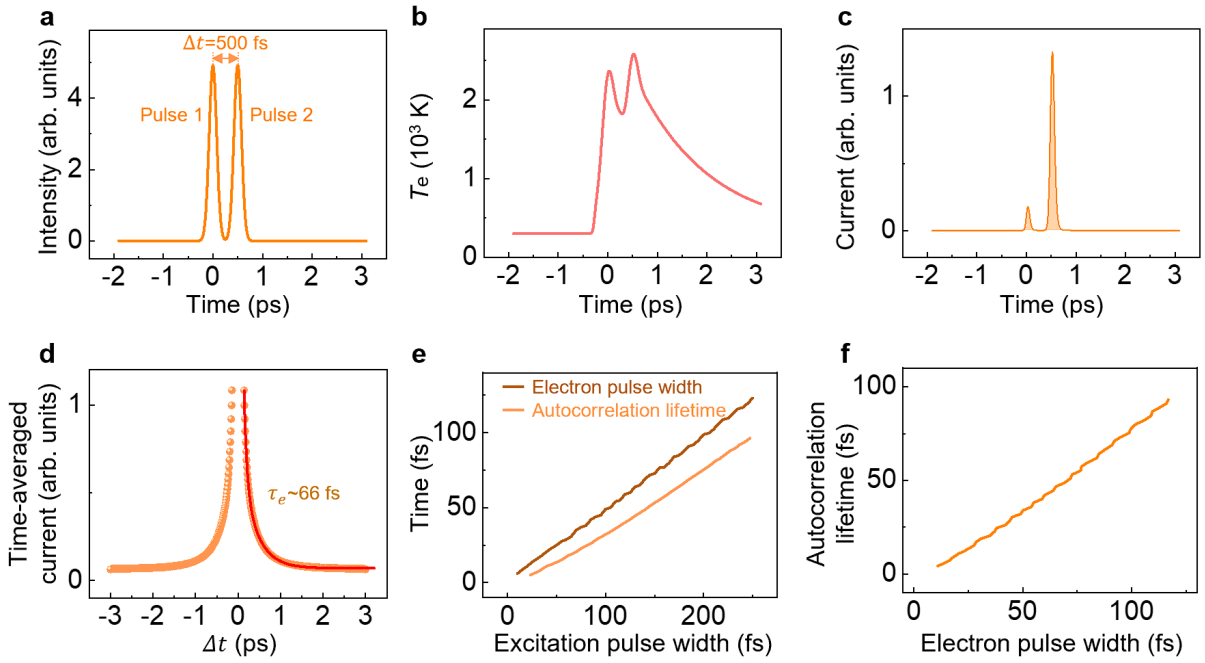
Supplementary Figure 5 | Pulse contrast evaluation. a, With excitation of 180 fs laser pulse, after about the first 200 fs (when T_e reaches an equilibrium with phonon temperature T_{ph}), there is a significant thermal lag in electron temperature. **b,** Resulting electron pulse as a function of time is compared with a Gaussian profile (FWHM = 85 fs) fitting. The thermal lag is greatly suppressed in electron pulse due to the highly nonlinear dependent of electron emission current on T_e. The pulse contrast is calculated $I_P = 1 - \frac{Thermal\ lag\ area}{Electron\ pulse\ area} = 96.2\%$. Therefore, the thermal lag in electron pulse can only induce a neglectable effect below 4%.



Supplementary Figure 6 | Autocorrelation setup for time-resolved PL and electron emission. Pulsed laser (~1.55 eV, 100 fs, 80 MHz) is divided into two parts with a tunable time delay Δt. Two pulses are combined together and then focused into optical fiber (YOFC CS-780). A proper length dispersion compensation fiber (NKT HC-800) is used to compress laser pulse width to ~180 fs. Optical fiber is sealed into a high vacuum chamber with a spectrometer and source meter to collect time delay-dependent photoluminescence and vacuum current. By varying time delay cross coincident point (-0.5 to 3 ps in this measurement), we can get both PL and vacuum current autocorrelation information.



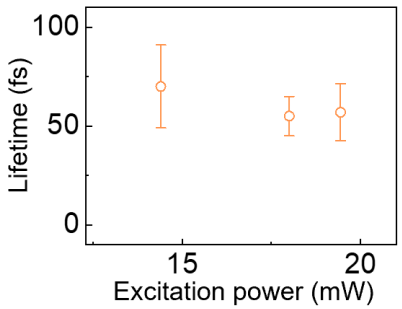
Supplementary Figure 7 | Accompanying ultrafast PL during electron emission from graphene. a, Time-resolved PL according to the evolvement of electron temperature. The full width at half maximum (FWHM) is ~140 fs. **b,** Autocorrelation measurement of photoluminescence with a derived lifetime (τ_{PL}) of ~130 fs, which agrees well with calculation results. Experimental data is acquired by optical fiber excitation at 800 nm with 19.4 mW.



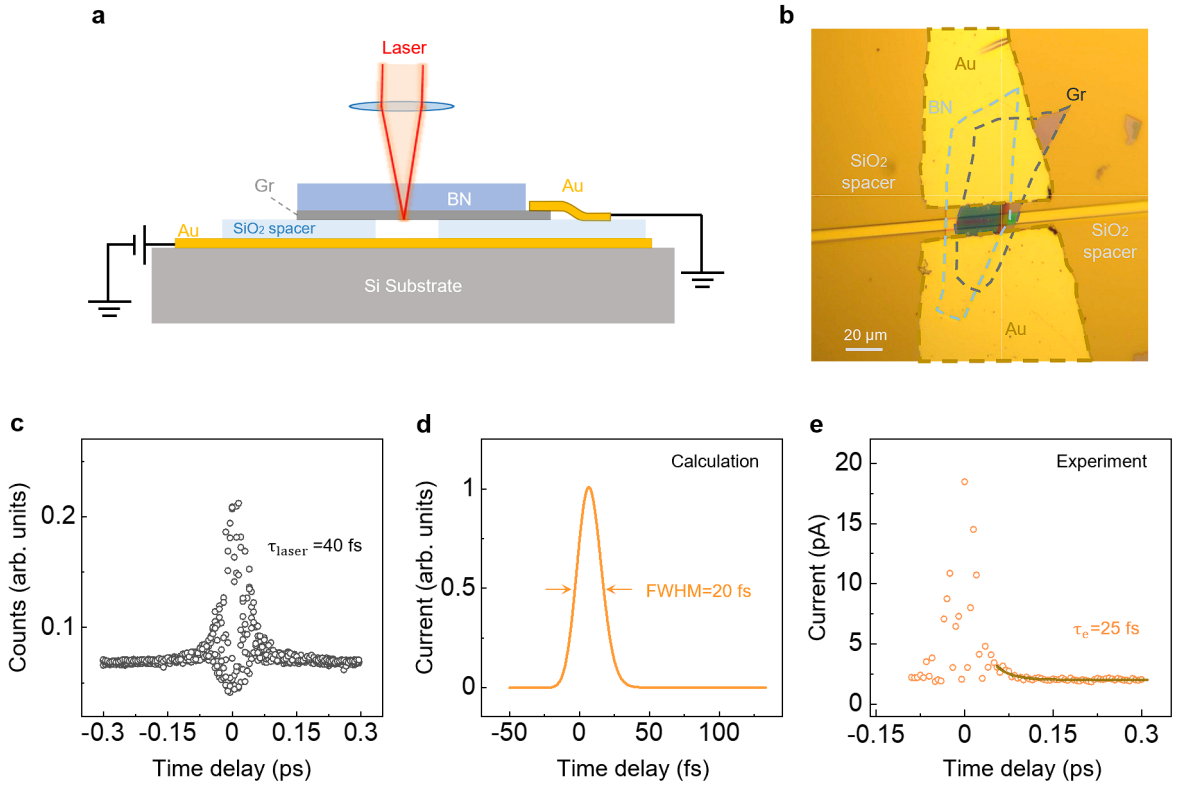
Supplementary Figure 8 | Relationship between autocorrelation lifetime and electron pulse width. a, Two-pulse (each with a pulse with of 180 fs) autocorrelation setup with a tunable time delay (Δt). 500 fs is set as an example, where total intensity composed of pulse 1 and pulse 2 is shown. **b,** Electron temperature evolution under two-pulse excitations, showing two separated temperature peaks. **c,** Hot electron emission current as a function of time under two-pulse excitations. Two separated current peaks are also observed due to the temperature behaviour. The real-time current is integrated over time to determine the time-averaged current. **d,** The time-averaged current (dots) as a function of time delay (Δt) and fitted with exponential decay (red line), showing a lifetime constant of ~66 fs. **e,** Predicted electron pulse width (calculated in Fig. 2d in main text) and predicted autocorrelation lifetime as a function of excitation pulse width, respectively. **f,** Relationship between autocorrelation lifetime and electron pulse width. The two parameters show a near-linear dependence.

In traditional bulk materials, the photoelectron emission process is usually described with three-step model: (i) Photon absorption, instantaneous process; (ii) Transportation to surface, tens of femtoseconds depending on material thickness; (iii) Escaping to vacuum, tens of attoseconds. Thus, electron transportation inside bulk material determines the overall lifetime of electron

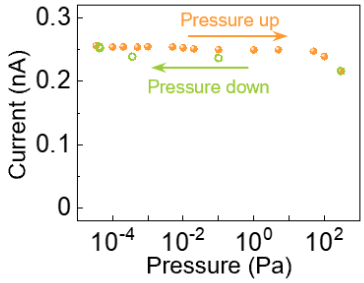
escaping time especially for back-illuminated devices. While in the condition of two-dimensional materials, the process of electron transportation to surface is neglectable, due to their atomic scale thickness. This is one of the figures of merits of two-dimensional materials for photoemission.



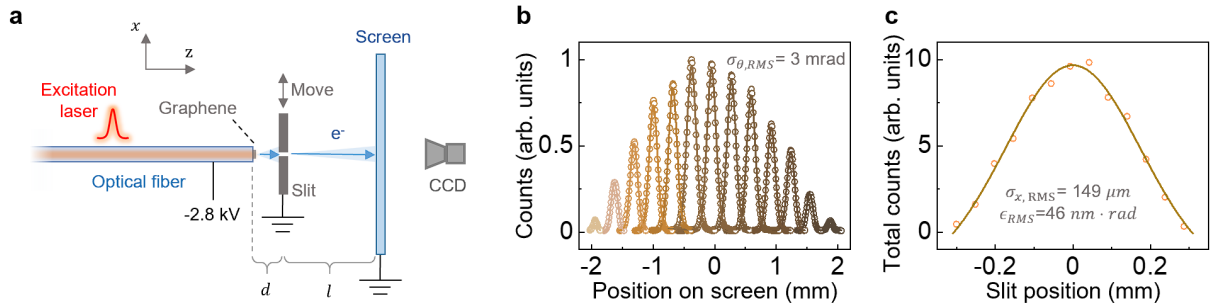
Supplementary Figure 9 | Autocorrelation lifetimes of electron emission under different excitation powers. The lifetimes keep near constant under different excitation powers. The error bars are from autocorrelation decay fitting standard error. All experiments are down with 800 nm optical fiber excitation.



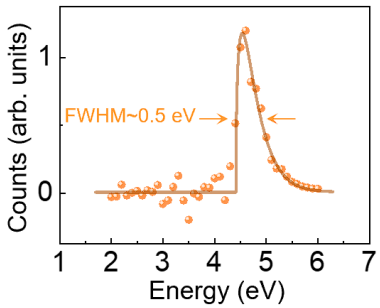
Supplementary Figure 10 | On-chip measurement of extreme pulse width of ultrafast graphene hot-electron emitter. a, Experiment setup of free space time-resolved electron emission of graphene. hBN encapsulated graphene is supported by 800 nm thick SiO_2 spacer as a photocathode. Gold film deposited on silicon substrate is set as anode. A proper voltage is applied to collect the emitted electrons from graphene. **b,** Optical microscope image of suspended graphene electron emission device. **c,** Optical autocorrelation measurement of excitation laser pulse width. Standard second harmonic generation (SHG) method is used. Tested pulse width (τ_{laser}) is ~40 fs. **d,** Calculated hot electron pulse width under 40 fs laser excitation. The result shows that FWHM of final pulse width is ~ 20 fs. **e,** Electron autocorrelation measurement of electron pulse width. Graphene is excited by 40 fs pulsed laser (1.55 eV with repetition rate of 80 MHz). The derived decay time is around 25 fs (corresponding to 40 fs electron pulse, according to Supplementary Figure 8) that matches calculation results well.



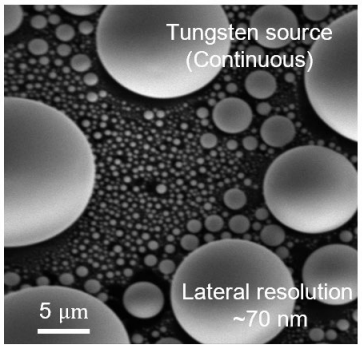
Supplementary Figure 11 | Emission current as a function of pressure during venting and pumping. After venting to ~300 Pa, molecular pump is activated to lower the pressure. When pressure is reduced back to ~4×10^{-5} Pa, emission current returned to almost the same level of previous value, showing excellent circumstance pressure tolerance. All data is acquired by optical fiber excitation at 1560 nm.



Supplementary Figure 12 | Emittance measurement. a, Single slit emittance measurement setups. A moveable 5 μm-width slit serves as a scanner to cut the electron beam at downstream from graphene with a distance of d=5 mm. The graphene electron emitter is biased with -2.8 kV for electron acceleration between photocathode and slit. The slit is grounded and scanned in x-axis. The screen equipped with a multichannel plate is also grounded to monitor the electron beam shape and intensity after the slit. The distance between slit and screen is l=25 mm. **b,** Electron beam patterns on screen at different slit positions (dots) with Gaussian fittings (solid lines). Each strip is integrated along y-axis. The typical FWHM of the strip at middle is ~0.176 mm. Therefore, the root mean square (RMS) angular spread ($\sigma_{\theta,RMS}$) is calculated as: $\sigma_{\theta,RMS} = 2 * tan^{-1}\left(\frac{0.176\ mm}{2*25\ mm*2.355}\right) = 3\ mrad.$ **c,** Integrated pattern intensities (circles) as a function of slit positions with Gaussian fitting (solid line). The FWHM is determined to be 350 μm, and the RMS beam width ($\sigma_{x,RMS}$) is calculated as 350 μm/2.355=149 μm. The normalized RMS emittance (ϵ_{RMS}) is calculated as: $\epsilon_{RMS} = \frac{p_z}{mc} \cdot \sigma_{\theta,RMS} \cdot \sigma_{x,RMS} = 46\ nm \cdot rad.$ p_z is electron momentum along z-axis, m is electron mass, c is light speed. Acceleration voltage is 2800 V.



Supplementary Figure 13 | Energy spectrum of electron beam emitted from graphene. The spectrum (dots) shows a thermionic emission behaviour with temperature of 2880 K and work function of 4.3 eV under 800 nm femtosecond laser excitation (peak intensity of ~2.2 GW/cm^2). FWHM of energy spectrum is about 0.5 eV. The fitting is according to thermionic electron emission function[2] (solid line).



Supplementary Figure 14 | Image quality comparation with a conventional source. Tabletop SEM imaging with original tungsten thermionic source. All parameters were set the same. The lateral resolution is determined to be ~70 nm compared to ~100 nm with our fiber integrated graphene ultrafast sources. It should be noted that the diminished lateral resolution in ultrafast electron source primarily results from increased noise, stemming from the low time-averaged current (a consequence of the ultrafast electron source's low duty cycle) when compared to a continuous source.

Supplementary Table 1 | Stabilities of ultrafast electron sources

Material	*Structure*	*Excitation wavelength (nm)*	*Mechanism*	*Duration (h)*	*Stability*	*Reference*
Graphene	Optical fiber-integration	1560	Hot electron emission	8	±0.5%	This work
Graphene	Optical fiber-integration	1560	Hot electron emission	150	±1%	This work
Graphene	Optical fiber-integration	1560	Hot electron emission	500	±5%	This work
LaB_6	Tip	257	Photoelectric	2.5	±4%	Ref.[3]
LaB_6	Tip	2250	Multiphoton	13	±3.75%	Ref.[4]
NCD-W	Tip	256	Photoelectric	0.4	±15%	Ref.[5]
NCD-W	Tip	512	Multiphoton	0.4	±10%	Ref.[5]
NCD-W	Tip	1932	Multiphoton	0.4	±9%	Ref.[5]
NCD-W	Tip	780	Multiphoton	13	±3%	Ref.[5]
ZrO_x-*W*	Tip	264	Photoelectric	6	±27%	Ref.[6]
Carbon nanotube	Tip	410	Optical field emission	50	±7%	Ref.[7]

Supplementary Table 2 | Parameters of optical fiber integrated graphene ultrafast electron source

Mean current	*Acceleration voltage*	*Energy spread*	*Angular spread*	*Source size*	*Normalized emittance*	*Peak reduced brightness*
10^{-9} *A*	2800 V	0.5 eV	3 mrad	4.5 μm	46 nm · rad	2.7×10^{4} A/($m^2 \cdot sr \cdot V$)

Supplementary Note 1: Theoretical two-temperature model for time-resolved electron emission from graphene.

Two-temperature model separates electron system and photon system of graphene and takes into consideration of their interaction after photoexcitation. The specific heat of electron system c_e and phonon system c_{ph} at different temperature T_e and T_{ph} can be described as

$$c_e(T_e) = \frac{21.6}{\pi(\hbar v_F)^2} k^3 T_e^2, \tag{S1}$$

$$c_{ph}(T_{ph}) = -4.79\times10^9 + 1.82\times10^7 T_{ph} + 1.34\times10^4 T_{ph}^2 + 5.16 T_{ph}^3, \tag{S2}$$

where v_F=*1.1×10^6 m/s* is Fermi velocity of graphene, k is Boltzmann constant.

After excitation of a gaussian shape laser pulse: $I(t) = \frac{F}{\sqrt{2\pi}\tau}\exp\left(\frac{-t^2}{2\tau^2}\right)$, F is absorbed fluence, τ presents duration of laser pulse. T_e increases sharply with an energy exchange with phonon system descripted as

$$\begin{aligned}\Gamma\left(T_e, T_{ph}\right) = \beta\Big\{&\left[1+n\left(T_{ph}\right)\right]\int D(E)D(E-\hbar\Omega)f\left(E,T_e\right)\left[1-f\left(E-\hbar\Omega,T_e\right)\right]dE \\ &-n\left(T_{ph}\right)\int D(E)D(E+\hbar\Omega)f\left(E,T_e\right)\left[1-f\left(E+\hbar\Omega,T_e\right)\right]dE\Big\},\end{aligned} \tag{S3}$$

where $D(E) = (2E/\pi)/\left(\hbar v_F\right)^2$ is density of states, $n\left(T_{ph}\right) = \left[\exp\left(\hbar\Omega/k_B T_{ph}\right)-1\right]^{-1}$ is phonon population distribution at temperature T_{ph}, $\hbar\Omega$=0.2 *eV* is optical phonon energy of graphene, β=*5 eV^{2}cm^{2}s^{-1}*. $f\left(E,T_e\right) = \left[\exp\left(E/k_B T_e\right)+1\right]^{-1}$ is Fermi-Dirac distribution at temperature T_e.

Based on this model, we can get the electron temperature as a function of time: $T_e(t)$. Time-resolved photoluminescence $PL(t)$ and hot-electron emission current $I_e(t)$ can be derived according to Plank's blackbody radiation law and Richardson-Dushman equation correspondingly:

$$PL(h\nu,t) = \frac{2h\nu^3}{c^2}\frac{1}{e^{h\nu/k_B T_e(t)}-1}, \tag{S4}$$

$$I_e(t) = C T_e(t)^2 \exp\left(-\frac{\phi}{k_B T_e(t)}\right). \tag{S5}$$

Supplementary Note 2: Brightness calculation

Based on the measured emittance in Fig. S12, the brightness (B) is calculated, assuming a symmetry in x and y direction of electron beam:

$$B = \frac{I}{\pi^2 \cdot \sigma_{\theta,RMS}^2 \cdot \sigma_{x,RMS}^2} = \frac{10^{-9}\, A}{\pi^2 \times (3\, mrad)^2 \times (149\ \mu m)^2} = 507\ \frac{A}{m^2 \cdot sr}. \quad \text{(S6)}$$

The time-averaged reduced brightness (B_r), which gives the brightness value without influence of acceleration voltage, is calculated as:

$$B_r = \frac{B}{V_r} = 0.18\ \frac{A}{m^2 \cdot sr \cdot V}, \quad \text{(S7)}$$

where V_r is acceleration voltage (without considering relativistic effect).

The peak reduced brightness ($B_{r,peak}$) is calculated considering the electron pulse width $\Gamma_e = 85\ fs$ and reputation rate R=80 MHz:

$$B_{r,peak} = \frac{B_r}{\Gamma_e \times R} = 2.7 \times 10^4\ \frac{A}{m^2 \cdot sr \cdot V}. \quad \text{(S8)}$$

Supplementary References

1. Yen, R., Liu, J. & Bloembergen, N. Thermally assisted multiphoton photoelectric emission from tungsten. *Optics Communications* **35**, 277–282 (1980).
2. McCarthy, P. T., Reifenberger, R. G. & Fisher, T. S. Thermionic and photo-excited electron emission for energy-conversion processes. *Front. Energy Res.* **2**, 54 (2014).
3. Yang, D.-S., Mohammed, O. F. & Zewail, A. H. Scanning ultrafast electron microscopy. *Proc. Natl. Acad. Sci. U.S.A.* **107**, 14993–14998 (2010).
4. Bhorade, O. *et al.* Bright and ultrafast electron point source made of LaB_6 nanotip. *Nanoscale Adv.* **5**, 2462–2469 (2023).
5. Tafel, A., Meier, S., Ristein, J. & Hommelhoff, P. Femtosecond laser-induced electron emission from nanodiamond-coated tungsten needle tips. *Phys. Rev. Lett.* **123**, 146802 (2019).
6. Kozák, M. *et al.* Ultrafast scanning electron microscope applied for studying the interaction between free electrons and optical near-fields of periodic nanostructures. *J. Appl. Phys.* **124**, 023104 (2018).
7. Li, C. *et al.* Carbon nanotubes as an ultrafast emitter with a narrow energy spread at optical frequency. *Adv. Mater.* **29**, 1701580 (2017).